

<https://helda.helsinki.fi>

Production of pi(0) and eta mesons in U plus U collisions at root S-NN=192 GeV

PHENIX Collaboration

2020-12-04

PHENIX Collaboration , Acharya , U , Kim , D J , Krizek , F , Novitzky , N & Rak , J 2020 , ' Production of pi(0) and eta mesons in U plus U collisions at root S-NN=192 GeV ' , Physical Review C , vol. 102 , no. 6 , 064905 . <https://doi.org/10.1103/PhysRevC.102.064905>

<http://hdl.handle.net/10138/325024>

<https://doi.org/10.1103/PhysRevC.102.064905>

cc_by

publishedVersion

Downloaded from Helda, University of Helsinki institutional repository.

This is an electronic reprint of the original article.

This reprint may differ from the original in pagination and typographic detail.

Please cite the original version.

Production of π^0 and η mesons in U+U collisions at $\sqrt{s_{NN}} = 192$ GeV

U. Acharya,²¹ C. Aidala,^{39,43} N. N. Ajitanand,^{62,*} Y. Akiba,^{57,58,†} R. Akimoto,¹¹ J. Alexander,⁶² K. Aoki,^{32,57} N. Apadula,^{28,63} H. Asano,^{35,57} E. T. Atomssa,⁶³ T. C. Awes,⁵³ B. Azmoun,⁷ V. Babintsev,²⁴ M. Bai,⁶ X. Bai,¹⁰ B. Bannier,⁶³ K. N. Barish,⁸ S. Bathe,^{5,58} V. Baublis,⁵⁵ C. Baumann,⁷ S. Baumgart,⁵⁷ A. Bazilevsky,⁷ M. Beaumier,⁸ R. Belmont,^{12,51,68} A. Berdnikov,⁶⁰ Y. Berdnikov,⁶⁰ L. Bichon,⁶⁸ D. Black,⁸ B. Blankenship,⁶⁸ D. S. Blau,^{34,48} J. S. Bok,⁵⁰ V. Borisov,⁶⁰ K. Boyle,⁵⁸ M. L. Brooks,³⁹ J. Bryslawskij,^{5,8} H. Buesching,⁷ V. Bumazhnov,²⁴ S. Butsyk,⁴⁹ S. Campbell,^{13,28} V. Canoa Roman,⁶³ C.-H. Chen,⁵⁸ C. Y. Chi,¹³ M. Chiu,⁷ I. J. Choi,²⁵ J. B. Choi,^{30,*} S. Choi,⁶¹ P. Christiansen,⁴⁰ T. Chujo,⁶⁷ V. Cianciolo,⁵³ B. A. Cole,¹³ M. Connors,²¹ N. Cronin,^{44,63} N. Crossette,⁴⁴ M. Csanád,¹⁶ T. Csörgő,⁷⁰ A. Datta,⁴⁹ M. S. Daugherty,¹ G. David,^{7,63} K. DeBlasio,⁴⁹ K. Dehmelt,⁶³ A. Denisov,²⁴ A. Deshpande,^{58,63} E. J. Desmond,⁷ L. Ding,²⁸ J. H. Do,⁷¹ L. D’Orazio,⁴¹ O. Drapier,³⁶ A. Drees,⁶³ K. A. Drees,⁴⁴ W. Fan,⁶³ D. E. Fields,⁴⁹ M. Finger,⁹ M. Finger, Jr.,⁹ D. Firak,¹⁵ R. Esha,⁶³ S. Esumi,⁶⁷ K. O. Eyser,⁷ B. Fadem,⁴⁴ W. Fan,⁶³ D. E. Fields,⁴⁹ M. Finger,⁹ M. Finger, Jr.,⁹ D. Firak,¹⁵ D. Fitzgerald,⁴³ F. Fleuret,³⁶ S. L. Fokin,³⁴ J. E. Frantz,⁵² A. Franz,⁷ A. D. Frawley,²⁰ Y. Fukao,³² T. Fusayasu,⁴⁶ K. Gainey,¹ C. Gal,⁶³ P. Garg,^{3,63} A. Garishvili,⁶⁵ I. Garishvili,³⁸ F. Giordano,²⁵ A. Glenn,³⁸ X. Gong,⁶² M. Gonin,³⁶ Y. Goto,^{57,59} R. Granier de Cassagnac,³⁶ N. Grau,² S. V. Greene,⁶⁸ M. Grosse Perdekamp,²⁵ Y. Gu,⁶² T. Gunji,¹¹ H. Guragain,²¹ T. Hachiya,^{47,58} J. S. Haggerty,⁷ K. I. Hahn,¹⁸ H. Hamagaki,¹¹ S. Y. Han,^{18,33} J. Hanks,⁶³ S. Hasegawa,²⁹ K. Hashimoto,^{57,59} R. Hayano,¹¹ X. He,²¹ T. K. Hemmick,⁶³ T. Hester,⁸ J. C. Hill,²⁸ A. Hodges,²¹ R. S. Hollis,⁸ K. Homma,²³ B. Hong,³³ T. Hoshino,²³ J. Huang,^{7,39} S. Huang,⁶⁸ T. Ichihara,^{57,58} Y. Ikeda,⁵⁷ K. Imai,²⁹ Y. Imazu,⁵⁷ M. Inaba,⁶⁷ A. Iordanova,⁸ D. Isenhower,¹ A. Isinhue,⁴⁴ D. Ivanishchev,⁵⁵ B. V. Jacak,⁶³ S. J. Jeon,⁴⁵ M. Jezghani,²¹ Z. Ji,⁶³ J. Jia,^{7,62} X. Jiang,³⁹ B. M. Johnson,^{7,21} K. S. Joo,⁴⁵ D. Jouan,⁵⁴ D. S. Jumper,²⁵ J. Kamin,⁶³ S. Kanda,^{11,32} B. H. Kang,²² J. H. Kang,⁷¹ J. S. Kang,²² J. Kapustinsky,³⁹ D. Kawall,⁴² A. V. Kazantsev,³⁴ J. A. Key,⁴⁹ V. Khachatryan,⁶³ P. K. Khandai,³ A. Khanzadeev,⁵⁵ A. Khatiwada,³⁹ K. M. Kijima,²³ C. Kim,³³ D. J. Kim,³¹ E.-J. Kim,³⁰ Y.-J. Kim,²⁵ Y. K. Kim,²² D. Kincses,¹⁶ E. Kistenev,⁷ J. Klatsky,²⁰ D. Kleinjan,⁸ P. Kline,⁶³ T. Koblesky,¹² M. Kofarago,^{16,70} B. Komkov,⁵⁵ J. Koster,⁵⁸ D. Kotchetkov,⁵² D. Kotov,^{55,60} F. Krizek,³¹ B. Kurygis,¹⁶ K. Kurita,⁵⁹ M. Kurosawa,^{57,58} Y. Kwon,⁷¹ R. Lacey,⁶² Y. S. Lai,¹³ J. G. Lajoie,²⁸ D. Larionova,⁶⁰ M. Larionova,⁶⁰ A. Lebedev,²⁸ D. M. Lee,³⁹ G. H. Lee,³⁰ J. Lee,^{18,64} K. B. Lee,³⁹ K. S. Lee,³³ S. H. Lee,^{28,43,63} M. J. Leitch,³⁹ M. Leitgab,²⁵ B. Lewis,⁶³ N. A. Lewis,⁴³ X. Li,¹⁰ X. Li,³⁹ S. H. Lim,^{12,56,71} M. X. Liu,³⁹ S. Lökös,¹⁶ D. Lynch,⁷ C. F. Maguire,⁶⁸ T. Majoros,¹⁵ Y. I. Makdisi,⁶ M. Makek,^{69,72} A. Manion,⁶³ V. I. Manko,³⁴ E. Mannel,⁷ M. McCumber,^{12,39} P. L. McGaughey,³⁹ D. McGlinchey,^{12,20,39} C. McKinney,²⁵ A. Meles,⁵⁰ M. Mendoza,⁸ B. Meredith,²⁵ W. J. Metzger,¹⁷ Y. Miake,⁶⁷ T. Mibe,³² A. C. Mignerey,⁴¹ A. Milov,⁶⁹ D. K. Mishra,⁴ J. T. Mitchell,⁷ Iu. Mitrakov,⁶⁰ S. Miyasaka,^{57,66} S. Mizuno,^{57,67} A. K. Mohanty,⁴ S. Mohapatra,⁶² T. Moon,³³ D. P. Morrison,⁷ S. I. Morrow,⁶⁸ M. Moskowicz,⁴⁴ T. V. Moukhanova,³⁴ B. Mulilo,^{33,57} T. Murakami,^{35,57} J. Murata,^{57,59} A. Mwai,⁶² T. Nagae,³⁵ S. Nagamiya,^{32,57} J. L. Nagle,¹² M. I. Nagy,¹⁶ I. Nakagawa,^{57,58} Y. Nakamiya,²³ K. R. Nakamura,^{35,57} T. Nakamura,⁵⁷ K. Nakano,^{57,66} C. Nattrass,⁶⁵ S. Nelson,¹⁹ P. K. Netrakanti,⁴ M. Nishashi,^{23,57} T. Niida,⁶⁷ R. Nouicer,^{7,58} T. Novák,^{17,70} N. Novitzky,^{31,63,67} A. S. Nyanin,³⁴ E. O’Brien,⁷ C. A. Ogilvie,²⁸ H. Oide,¹¹ K. Okada,⁵⁸ J. D. Osborn,⁴³ A. Oskarsson,⁴⁰ K. Ozawa,^{32,67} R. Pak,⁷ V. Pantuev,²⁶ V. Papavassiliou,⁵⁰ I. H. Park,^{18,64} S. Park,^{61,63} S. K. Park,³³ S. F. Pate,⁵⁰ L. Patel,²¹ M. Patel,²⁸ J.-C. Peng,²⁵ W. Peng,⁶⁸ D. V. Perepelitsa,^{12,13} G. D. N. Perera,⁵⁰ D. Yu. Peressounko,³⁴ C. E. PerezLara,⁶³ J. Perry,²⁸ R. Petti,^{7,63} C. Pinkenbun,⁷ R. P. Pisani,⁷ M. Potekhin,⁷ A. Pun,^{50,52} M. L. Purschke,⁷ H. Qu,¹ P. V. Radzevich,⁶⁰ J. Rak,³¹ N. Ramasubramanian,⁶³ I. Ravinovich,⁶⁹ K. F. Read,^{53,65} D. Reynolds,⁶² V. Riabov,^{48,55} Y. Riabov,^{55,60} E. Richardson,⁴¹ D. Richford,⁵ T. Rinn,^{25,28} N. Riveli,⁵² D. Roach,⁶⁸ S. D. Rolnick,⁸ M. Rosati,²⁸ J. Runchey,²⁸ M. S. Ryu,²² B. Sahlmueller,⁶³ N. Saito,³² T. Sakaguchi,⁷ H. Sako,²⁹ V. Samsonov,^{48,55} M. Sarsour,²¹ S. Sato,²⁹ S. Sawada,³² K. Sedgwick,⁸ J. Seele,⁵⁸ R. Seidl,^{57,58} Y. Sekiguchi,¹¹ A. Sen,^{21,28} R. Seto,⁸ P. Sett,⁴ D. Sharma,⁶³ A. Shaver,²⁸ I. Shein,²⁴ T.-A. Shibata,^{57,66} K. Shigaki,²³ M. Shimomura,^{28,47} K. Shoji,⁵⁷ P. Shukla,⁴ A. Sickles,^{7,25} C. L. Silva,³⁹ D. Silvermyr,^{40,53} B. K. Singh,³ C. P. Singh,³ V. Singh,³ M. Skolnik,⁴⁴ M. Slunečka,⁹ K. L. Smith,²⁰ S. Solano,⁴⁴ R. A. Soltz,³⁸ W. E. Sondheim,³⁹ S. P. Sorensen,⁶⁵ I. V. Sourikova,⁷ P. W. Stankus,⁵³ P. Steinberg,⁷ E. Stenlund,⁴⁰ M. Stepanov,^{42,*} A. Ster,⁷⁰ S. P. Stoll,⁷ M. R. Stone,¹² T. Sugitate,²³ A. Sukhanov,⁷ J. Sun,⁶³ X. Sun,²¹ Z. Sun,¹⁵ A. Takahara,¹¹ A. Taketani,^{57,58} Y. Tanaka,⁴⁶ K. Tanida,^{29,58,61} M. J. Tannenbaum,⁷ S. Tarafdar,^{3,68} A. Taranenko,^{48,62} E. Tennant,⁵⁰ A. Timilsina,²⁸ T. Todoroki,^{57,58,67} M. Tomášek,^{14,27} H. Torii,¹¹ R. S. Towell,¹ I. Tserruya,⁶⁹ Y. Ueda,²³ B. Ujvari,¹⁵ H. W. van Hecke,³⁹ M. Vargyas,^{16,70} E. Vazquez-Zambrano,¹³ A. Veicht,¹³ J. Velkovska,⁶⁸ R. Vértesi,⁷⁰ M. Virius,¹⁴ V. Vrba,^{14,27} E. Vznuzdaev,⁵⁵ X. R. Wang,^{50,58} D. Watanabe,²³ K. Watanabe,^{57,59} Y. Watanabe,^{57,58} Y. S. Watanabe,^{11,32} F. Wei,⁵⁰ S. Whitaker,²⁸ S. Wolin,²⁵ C. P. Wong,²¹

*Deceased.

†akiba@rcf.rhic.bnl.gov

C. L. Woody,⁷ Y. Wu,⁸ M. Wysocki,⁵³ B. Xia,⁵² Q. Xu,⁶⁸ Y. L. Yamaguchi,^{11,63} A. Yanovich,²⁴ S. Yokkaichi,^{57,58} I. Yoon,⁶¹ Z. You,³⁹ I. Younus,^{37,49} I. E. Yushmanov,³⁴ W. A. Zajc,¹³ A. Zelenski,⁶ Y. Zhai,²⁸ S. Zharko,⁶⁰ S. Zhou,¹⁰ and L. Zou⁸
(PHENIX Collaboration)

¹Abilene Christian University, Abilene, Texas 79699, USA

²Department of Physics, Augustana University, Sioux Falls, South Dakota 57197, USA

³Department of Physics, Banaras Hindu University, Varanasi 221005, India

⁴Bhabha Atomic Research Centre, Bombay 400 085, India

⁵Baruch College, City University of New York, New York, New York, 10010 USA

⁶Collider-Accelerator Department, Brookhaven National Laboratory, Upton, New York 11973-5000, USA

⁷Physics Department, Brookhaven National Laboratory, Upton, New York 11973-5000, USA

⁸University of California-Riverside, Riverside, California 92521, USA

⁹Charles University, Ovocný trh 5, Praha 1, 116 36, Prague, Czech Republic

¹⁰Science and Technology on Nuclear Data Laboratory, China Institute of Atomic Energy, Beijing 102413, People's Republic of China

¹¹Center for Nuclear Study, Graduate School of Science, University of Tokyo, 7-3-1 Hongo, Bunkyo, Tokyo 113-0033, Japan

¹²University of Colorado, Boulder, Colorado 80309, USA

¹³Columbia University, New York, New York 10027 and Nevis Laboratories, Irvington, New York 10533, USA

¹⁴Czech Technical University, Zikova 4, 166 36 Prague 6, Czech Republic

¹⁵Debrecen University, H-4010 Debrecen, Egyetem tér 1, Hungary

¹⁶ELTE, Eötvös Loránd University, H-1117 Budapest, Pázmány P. s. 1/A, Hungary

¹⁷Eszterházy Károly University, Károly Róbert Campus, H-3200 Gyöngyös, Mátrai út 36, Hungary

¹⁸Ewha Womans University, Seoul 120-750, Korea

¹⁹Florida A&M University, Tallahassee, Florida 32307, USA

²⁰Florida State University, Tallahassee, Florida 32306, USA

²¹Georgia State University, Atlanta, Georgia 30303, USA

²²Hanyang University, Seoul 133-792, Korea

²³Hiroshima University, Kagamiyama, Higashi-Hiroshima 739-8526, Japan

²⁴IHEP Protvino, State Research Center of Russian Federation, Institute for High Energy Physics, Protvino, 142281, Russia

²⁵University of Illinois at Urbana-Champaign, Urbana, Illinois 61801, USA

²⁶Institute for Nuclear Research of the Russian Academy of Sciences, prospekt 60-letiya Oktyabrya 7a, Moscow 117312, Russia

²⁷Institute of Physics, Academy of Sciences of the Czech Republic, Na Slovance 2, 182 21 Prague 8, Czech Republic

²⁸Iowa State University, Ames, Iowa 50011, USA

²⁹Advanced Science Research Center, Japan Atomic Energy Agency, 2-4 Shirakata Shirane, Tokai-mura, Naka-gun, Ibaraki-ken 319-1195, Japan

³⁰Jeonbuk National University, Jeonju, 54896, Korea

³¹Helsinki Institute of Physics and University of Jyväskylä, P.O.Box 35, FI-40014 Jyväskylä, Finland

³²KEK, High Energy Accelerator Research Organization, Tsukuba, Ibaraki 305-0801, Japan

³³Korea University, Seoul, 02841, Korea

³⁴National Research Center "Kurchatov Institute," Moscow, 123098 Russia

³⁵Kyoto University, Kyoto 606-8502, Japan

³⁶Laboratoire Leprince-Ringuet, Ecole Polytechnique, CNRS-IN2P3, Route de Saclay, F-91128, Palaiseau, France

³⁷Physics Department, Lahore University of Management Sciences, Lahore 54792, Pakistan

³⁸Lawrence Livermore National Laboratory, Livermore, California 94550, USA

³⁹Los Alamos National Laboratory, Los Alamos, New Mexico 87545, USA

⁴⁰Department of Physics, Lund University, Box 118, SE-221 00 Lund, Sweden

⁴¹University of Maryland, College Park, Maryland 20742, USA

⁴²Department of Physics, University of Massachusetts, Amherst, Massachusetts 01003-9337, USA

⁴³Department of Physics, University of Michigan, Ann Arbor, Michigan 48109-1040, USA

⁴⁴Muhlenberg College, Allentown, Pennsylvania 18104-5586, USA

⁴⁵Myongji University, Yongin, Kyonggido 449-728, Korea

⁴⁶Nagasaki Institute of Applied Science, Nagasaki-shi, Nagasaki 851-0193, Japan

⁴⁷Nara Women's University, Kita-uoya Nishi-machi Nara 630-8506, Japan

⁴⁸National Research Nuclear University, MEPhI, Moscow Engineering Physics Institute, Moscow, 115409, Russia

⁴⁹University of New Mexico, Albuquerque, New Mexico 87131, USA

⁵⁰New Mexico State University, Las Cruces, New Mexico 88003, USA

⁵¹Physics and Astronomy Department, University of North Carolina at Greensboro, Greensboro, North Carolina 27412, USA

⁵²Department of Physics and Astronomy, Ohio University, Athens, Ohio 45701, USA

⁵³Oak Ridge National Laboratory, Oak Ridge, Tennessee 37831, USA

⁵⁴IPN-Orsay, Univ. Paris-Sud, CNRS/IN2P3, Université Paris-Saclay, BPI, F-91406, Orsay, France

⁵⁵PNPI, Petersburg Nuclear Physics Institute, Gatchina, Leningrad region, 188300, Russia

⁵⁶Pusan National University, Pusan 46241, Korea

⁵⁷RIKEN Nishina Center for Accelerator-Based Science, Wako, Saitama 351-0198, Japan

⁵⁸RIKEN BNL Research Center, Brookhaven National Laboratory, Upton, New York 11973-5000, USA

⁵⁹Physics Department, Rikkyo University, 3-34-1 Nishi-Ikebukuro, Toshima, Tokyo 171-8501, Japan

⁶⁰Saint Petersburg State Polytechnic University, St. Petersburg, 195251 Russia

⁶¹Department of Physics and Astronomy, Seoul National University, Seoul 151-742, Korea

⁶²Chemistry Department, Stony Brook University, SUNY, Stony Brook, New York 11794-3400, USA

⁶³Department of Physics and Astronomy, Stony Brook University, SUNY, Stony Brook, New York 11794-3800, USA

⁶⁴Sungkyunkwan University, Suwon, 440-746, Korea

⁶⁵University of Tennessee, Knoxville, Tennessee 37996, USA

⁶⁶Department of Physics, Tokyo Institute of Technology, Oh-okayama, Meguro, Tokyo 152-8551, Japan

⁶⁷Tomonaga Center for the History of the Universe, University of Tsukuba, Tsukuba, Ibaraki 305, Japan

⁶⁸Vanderbilt University, Nashville, Tennessee 37235, USA

⁶⁹Weizmann Institute, Rehovot 76100, Israel

⁷⁰Institute for Particle and Nuclear Physics, Wigner Research Centre for Physics, Hungarian Academy of Sciences (Wigner RCP, RMKI)

H-1525 Budapest 114, POBox 49, Budapest, Hungary

⁷¹Yonsei University, IPAP, Seoul 120-749, Korea

⁷²Department of Physics, Faculty of Science, University of Zagreb, Bijenička c. 32 HR-10002 Zagreb, Croatia



(Received 2 June 2020; accepted 9 November 2020; published 4 December 2020)

The PHENIX experiment at the Relativistic Heavy Ion Collider measured π^0 and η mesons at midrapidity in U + U collisions at $\sqrt{s_{NN}} = 192$ GeV in a wide transverse momentum range. Measurements were performed in the $\pi^0(\eta) \rightarrow \gamma\gamma$ decay modes. A strong suppression of π^0 and η meson production at high transverse momentum was observed in central U + U collisions relative to binary scaled $p + p$ results. Yields of π^0 and η mesons measured in U + U collisions show similar suppression pattern to those measured in Au + Au collisions at $\sqrt{s_{NN}} = 200$ GeV for similar numbers of participant nucleons. The η/π^0 ratios do not show dependence on centrality or transverse momentum and are consistent with previously measured values in hadron-hadron, hadron-nucleus, nucleus-nucleus, and e^+e^- collisions.

DOI: [10.1103/PhysRevC.102.064905](https://doi.org/10.1103/PhysRevC.102.064905)

I. INTRODUCTION

Extensive studies of heavy-ion collisions (A + A) at the Relativistic Heavy Ion Collider (RHIC) resulted in the discovery of the quark-gluon plasma (QGP) [1–4]. Subsequent measurements at the Large Hadron Collider [5–8] confirmed the suppression of high- p_T hadrons characteristic of the QGP and firmly established the existence of true jet quenching. Since then, one of the main efforts of RHIC experiments was directed towards detailed studies of the properties of the new state of nuclear matter, in part by making more differential and more precise measurements, but also by varying the collision energy and system size. The culmination of the latter was colliding U + U, the largest ever nucleus-nucleus collision system studied so far at RHIC or the Large Hadron Collider.

Creation of the QGP causes a variety of observable effects, including the so-called jet-quenching [9–11], which manifests itself by strongly suppressed production of high transverse momentum (p_T) hadrons in A + A, relative to the yields measured in proton-proton ($p + p$) collisions and scaled by the number of expected binary nucleon-nucleon collisions. The suppression is related to the energy loss of hard-scattered partons in a quark-gluon medium via bremsstrahlung and elastic scatterings. Parton energy loss is characterized by the \hat{q} transport parameter, which represents the squared four-

momentum transfer between the parton and the medium per unit path length and carries information on the medium coupling [10,12]. Values of the \hat{q} parameter cannot yet be estimated from first principles. Instead, several phenomenological jet-quenching models [13–17] exist, all based on experimental results.

Quantitatively, medium effects in A + A are usually characterized with the nuclear modification factor (R_{AA}):

$$R_{AA}^{\text{cent}}(p_T) = \frac{1}{T_{AA}^{\text{cent}}} \frac{dN_{AA}^{\text{cent}}/dp_T}{d\sigma_{pp}/dp_T}, \quad (1)$$

where $dN_{AA}^{\text{cent}}/dp_T$ is the particle yield measured in A + A collisions for a given centrality class (cent), $d\sigma_{pp}/p_T$ is the particle production cross section measured in $p + p$ collisions at the same collision energy while T_{AA}^{cent} is the nuclear thickness function for the event centrality class [18].

Measurements of the production of different types of mesons allow a systematic study of jet quenching with respect to the fragmentation function and quantum numbers (mass, flavor, spin, etc.) of the final-state hadrons. For example, π^0 mesons contain only the first generation quarks (u, d) and thus are produced abundantly, while η mesons have a hidden strangeness content and four times larger mass than π^0 . Measurement of the η/π^0 ratios in A + A gives an opportunity to

better understand the possible changes of parton fragmentation mechanisms with respect to system size, collision energy, and geometry. They are also an important input for the measurement of direct photons.

In this paper we present results on π^0 and η meson p_T invariant yields, R_{AA} , and η/π^0 ratios in U + U collisions at $\sqrt{s_{NN}} = 192$ GeV. The $^{238}\text{U} + ^{238}\text{U}$ is the largest collision system at RHIC, reaching the highest energy density central collisions [19]. In contrast with the nearly or completely spherical geometries of the Cu, Au, and Pb nuclei [5–7,20–26], ^{238}U is highly deformed. This feature makes U + U collisions particularly interesting for jet-quenching studies. However, when comparing physics observables in U + U with Cu + Cu, Au + Au, or Pb + Pb collisions, one has to be aware that, in any finite collision centrality bin, the fluctuations of the overlap volume and energy density are larger in U + U than in the case of spherical nuclei.

II. DATA ANALYSIS

All results presented in this paper were obtained with the PHENIX spectrometer from data collected in the Year-2012 data taking period at RHIC. A detailed description of the PHENIX experimental setup can be found elsewhere [27]. Event selection is performed with two beam-beam counters (BBCs) [28] located towards the north and south beam directions in the $3.0 < |\eta| < 3.9$ pseudorapidity interval. The collision vertex coordinate along the beam direction (z_{BBC}) is determined by the time difference between two hits in the north and south BBCs with an accuracy of 0.6–2 cm (depending on the particle multiplicity). The analyzed data set was taken with the minimum-bias (MB) trigger, which required a north-south coincidence and an online vertex position within ± 30 cm. After offline reconstruction an additional cut of $|z_{\text{BBC}}| < 20$ cm was applied; the remaining data set comprises 9.4×10^8 events.

The event centrality is derived from the distribution of the total charge in the BBCs. For each centrality class the mean values of the collision geometry parameters, such as the number of binary inelastic collisions (N_{coll}), participating nucleons (N_{part}), and T_{AA} (the nuclear overlap integral) are determined by using a Glauber model based Monte Carlo simulation of BBC charge response [18]. For asymmetric ^{238}U nuclei the θ -dependent Woods-Saxon density distribution is used:

$$\rho(r, \theta)/\rho_0 = \frac{1}{1 + \exp\{[r - R'(\theta)]/a\}}, \quad (2)$$

where ρ_0 is the density at the center of the nucleus, a is the diffusion parameter, $R'(\theta) = R[1 + \beta_2 Y_2^0(\theta) + \beta_4 Y_4^0(\theta)]$, and $Y_2^0(\theta)$ and $Y_4^0(\theta)$ are the Legendre polynomials. Because there is no single universally accepted parametrization of the U + U nucleus, we followed the example of Refs. [29,30] and used the same two parameter sets. Accordingly, two Monte Carlo simulations were produced incorporating different parametrizations of $R'(\theta)$ (see Table I) and, thus, two sets (Glauber 1 [31] and Glauber 2 [32]) of collision-geometry parameters are used, listed in Table II. The obtained N_{part} values are the same in central collisions and are slightly different in more peripheral collisions. When comparing hadron yields

TABLE I. Parameters for the Woods-Saxon distributions used for U + U Glauber Monte Carlo simulations.

Parameter	Glauber 1 [31]	Glauber 2 [32]
R (fm)	6.81	6.86
a (fm)	0.60	0.42
β_2	0.280	0.265
β_4	0.093	0

or R_{AA} between U + U and Au + Au collisions at centralities with similar N_{part} we have to keep in mind that the rms of the N_{part} distribution is wider in U + U than in Au + Au.

Invariant yields of π^0 and η mesons are obtained from

$$\frac{1}{N_{\text{event}}} \frac{d^2 N}{2\pi p_T dp_T dy} = \frac{N_{\text{raw}}}{2\pi p_T N_{\text{event}} \epsilon_{\text{rec}} \Delta p_T \Delta y}, \quad (3)$$

where N_{raw} is the particle raw yield, ϵ_{rec} is the efficiency (including acceptance and all other corrections), and N_{event} is the number of analyzed events.

The π^0 and η mesons were reconstructed via the $\pi^0 \rightarrow \gamma\gamma$ and $\eta \rightarrow \gamma\gamma$ decay channels using the electromagnetic calorimeter (EMCal) [33]. The EMCal comprises two technologically different subsystems: lead-scintillator sampling calorimeter (PbSc) in four sectors in the west and two sectors in the east PHENIX arms, and lead-glass Čerenkov calorimeter (PbGl) in two sectors in the east PHENIX arm. Each sector covers $|\eta| < 0.35$ pseudorapidity range and 22.5 degrees in azimuth. The subsystems have different nonlinearity, energy resolution ($\delta E/E = 2.1\% \oplus 8.1\%/\sqrt{E}$ for PbSc and $0.8\% \oplus 5.9\%/\sqrt{E}$ for PbGl) and segmentation ($\delta\phi \times \delta\eta \approx 0.01 \times 0.01$ for PbSc and 0.008×0.008 for PbGl).

Showers in the EMCal are selected as γ candidates if they pass a shower shape cut [33] and a minimum-energy cut ($E_{\gamma \text{ min}} = 0.4$ GeV) to reduce contamination from minimum ionizing hadrons. Then $\gamma\gamma$ pairs are formed from all photon candidates in the same sector under the condition

TABLE II. The mean values of $\langle T_{AA} \rangle$ and the mean number of participating nucleons $\langle N_{\text{part}} \rangle$ in different U + U centrality intervals. The values are shown with their systematic uncertainties, estimated by varying different input parameters and by using different nucleon density profiles in the Monte Carlo Glauber simulations.

Glauber	Centrality interval	$\langle T_{AA} \rangle$ (mb $^{-1}$)	$\langle N_{\text{part}} \rangle$
Glauber 1 [31]	Minimum Bias	8.2 ± 1.6	143 ± 5
	0%–20%	22.1 ± 2.3	330 ± 6
	20%–40%	7.9 ± 0.8	159 ± 7
	40%–60%	2.3 ± 0.3	64.8 ± 5.9
	60%–80%	0.41 ± 0.09	17.8 ± 3.2
Glauber 2 [32]	Minimum Bias	8.9 ± 1.0	144 ± 5
	0%–20%	23.7 ± 2.7	330 ± 6
	20%–40%	8.9 ± 1.1	161 ± 7
	40%–60%	2.6 ± 0.4	65.8 ± 5.8
	60%–80%	0.47 ± 0.10	18.2 ± 3.2
	40%–80%	1.54 ± 0.22	42.0 ± 4.5

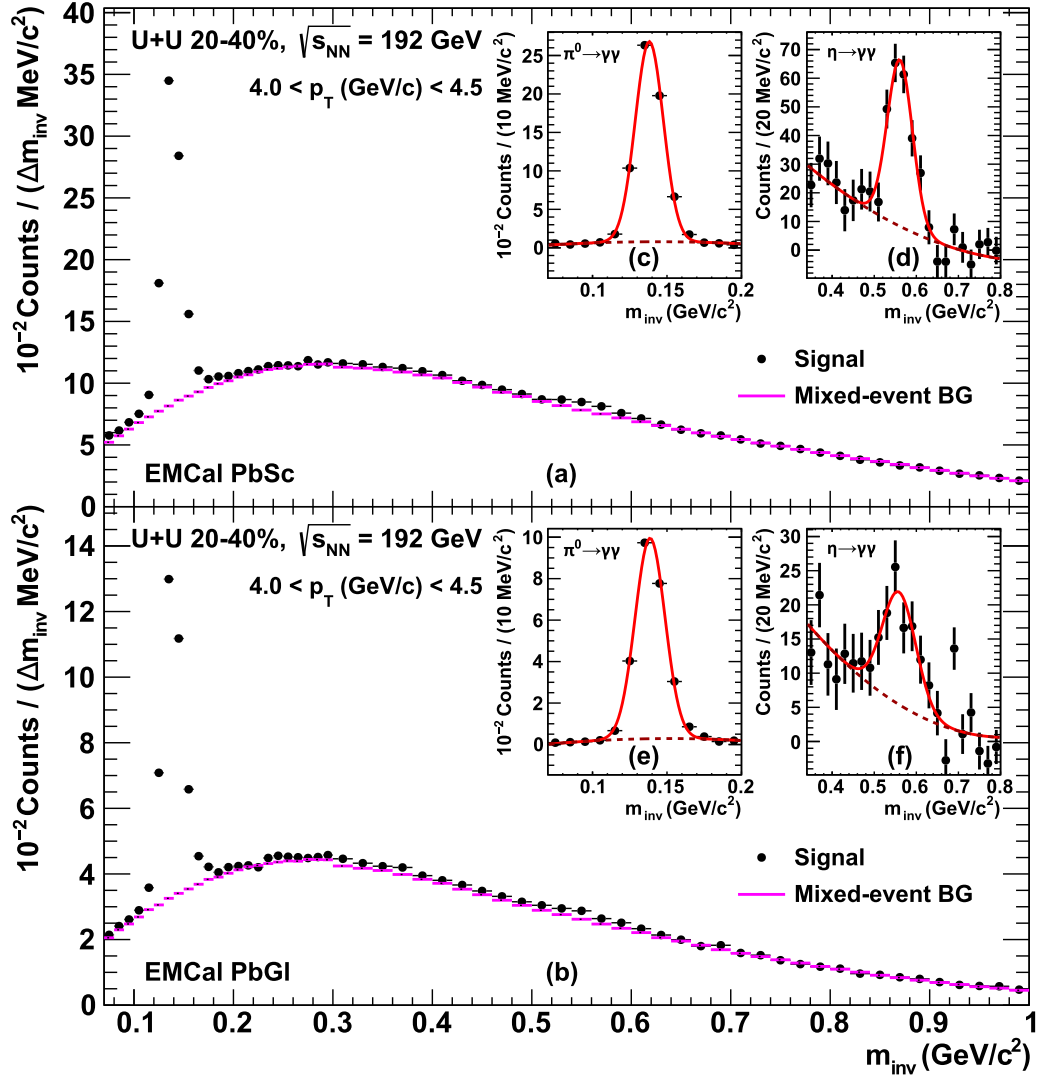


FIG. 1. Invariant-mass distributions for $\gamma\gamma$ pairs, obtained in 4–4.5 GeV/c p_T interval in 20%–40% centrality U + U collisions. Panels (a) and (b) show the signal and normalized mixed-event background invariant-mass distributions in PbSc and PbGl subsystems, respectively. In label captions, Δm_{inv} stands for the invariant-mass bin width and is equal to 10 MeV/c^2 for $m_{\text{inv}} < 0.3$ GeV/c^2 and for 20 MeV/c^2 at larger m_{inv} values. Inserts (c) and (d) show the invariant-mass distributions in π^0 and η regions after the mixed-event background subtraction in PbSc, while inserts (e) and (f) show ones in PbGl.

that their energies ($E_{\gamma 1}$ and $E_{\gamma 2}$) satisfy an asymmetry cut $|E_{\gamma 1} - E_{\gamma 2}| / (E_{\gamma 1} + E_{\gamma 2}) < 0.8$ to reduce the combinatorial background.

To determine raw yields of π^0 and η mesons the invariant-mass (m_{inv}) distributions of $\gamma\gamma$ pairs passing the cuts are produced in different p_T and centrality intervals, separately for PbSc and PbGl subsystems [20]. The distributions contain a background and two signal peaks around $m_{\text{inv}} \approx 0.14$ and 0.55 GeV/c^2 , corresponding to π^0 and η decays, respectively. The background comprises correlated and uncorrelated components. The correlated component comes from photons of other particle decays (K_S , ω , ρ , η' , etc.). The uncorrelated component of the background comes from combinations of uncorrelated γ candidates and is well reproduced by event mixing, where $\gamma\gamma$ pairs are formed from two γ candidates from different events with similar collision vertex (z_{BEC}) and centrality. Estimated background shapes are normalized to

the real (same-event) $\gamma\gamma$ m_{inv} distributions in the ranges $0.08 < m_{\text{inv}} < 0.085$ and $0.36 < m_{\text{inv}} < 0.40$ GeV/c^2 for the π^0 , in $0.7 < m_{\text{inv}} < 0.8$ GeV/c^2 for the η , and then subtracted. Due to the rapid decrease of the combinatorial background with increasing p_T , the mixed-event subtraction is implemented only for $p_T < 10$ GeV/c . Typical $\gamma\gamma$ invariant-mass distributions and corresponding normalized mixed-event background shapes are presented in Fig. 1, where panels (a) and (b) correspond to PbSc and PbGl measurements, respectively. Note that, in Fig. 1, the foreground and background distributions plotted at $m_{\text{inv}} < 0.3$ GeV/c^2 correspond to π^0 meson measurement, while at higher m_{inv} values ones correspond to η measurements, so the distributions have different bin width in the two invariant-mass ranges.

The resulting m_{inv} distributions are fit to a combination of a Gaussian and a polynomial to describe a signal and the residual (correlated) background, respectively. For π^0

TABLE III. Sources of systematic uncertainties for π^0 and η yields at different p_T . Values are shown for PbSc(PbGl) subsystems. The types of uncertainties are described in the text. Values with a range indicate the variation of the uncertainty over the different centrality intervals.

Yield	Source	2.75 GeV/c	13 GeV/c	Type
$\pi^0 \rightarrow \gamma\gamma$	Acceptance	1.5%(1.5%)	1.5%(1.5%)	B
	p_T weights	1%(1%)	1%(1%)	B
	Energy scale	5%(5%)	7%(7%)	B
	Energy resolution	2%(2%)	2%(2%)	B
	Photon conversion	5.2%(5.2%)	5.2%(5.2%)	C
	Cluster merging		7%(4%)	B
	PID cuts	1.6%(4%)–4%(4%)	4%(4%)–6%(4%)	B
	Raw yield extraction	1%(1%)–3%(2%)	2%(2%)	B
	Reconstruction efficiency	0.8%(1.3%)–1.3%(2.0%)	0.3%(0.4%)–0.4%(0.8%)	A
$\eta \rightarrow \gamma\gamma$	Acceptance	1.5%(1.5%)	1.5%(1.5%)	B
	p_T weights	1%(1%)	1%(1%)	B
	Energy scale	3%(3%)	6%(6%)	B
	Energy resolution	2%(2%)	2%(2%)	B
	Photon conversion	5.2%(5.2%)	5.2%(5.2%)	C
	PID cuts	5%(5%)–5%(7%)	5%(5%)	B
	Raw yield extraction	11%(11%)	8%(8%)	B
	Reconstruction efficiency	1.2%(2.5%)–3%(5.4%)	0.4%(0.7%)–0.9%(1.4%)	A

and η measurements, respectively, first- and second-order polynomials were used. Meson raw yields are determined as the difference between the integrals of the bin content and the polynomial in the mass peak regions, which are defined as $0.10 < m_{\text{inv}} < 0.17$ and $0.48 < m_{\text{inv}} < 0.62$ GeV/ c^2 for π^0 and η peaks, respectively. Figures 1(c)–1(f) present examples of the resulting m_{inv} distributions in the π^0 [Figs. 1(c) and 1(e)] and η [Figs. 1(e) and 1(f)] regions obtained in PbSc [Figs. 1(c) and 1(d)] or PbGl Figs. 1(e) and 1(f) subsystems as well as the corresponding fitting functions examples.

Acceptance and reconstruction efficiency (efficiency hereafter) is estimated by using a GEANT3-based [34] Monte Carlo simulation of the PHENIX detector. The simulation is tuned to reproduce the observed mass peaks and widths of π^0 and η mesons in the real data. To account for the effect of underlying events (multiplicity) the simulated mesons are embedded in real data in each centrality, then analyzed with the same methods as the real data. Final efficiencies also account for branching ratios of the meson decay modes.

Systematic uncertainties of the measurements are classified into three types. Type-A uncertainties are entirely p_T uncorrelated and are added in quadrature to the statistical uncertainties. Type-B uncertainties are p_T correlated, but different from point to point, and all data points can move up or down by the same fraction of their type-B uncertainty. Type-C uncertainties move all points up or down by the same fraction [35].

Sources of systematic uncertainties for π^0 and η yield measurements are listed in Table III for representative p_T values. Examples of total uncertainties of different types for the meson spectra, R_{AA} , and ratios are listed in Table IV.

In π^0 measurements, the main sources of systematic uncertainty at low p_T (1–3 GeV/ c) are photon conversions in the detector material, at intermediate p_T (3–12 GeV/ c) the absolute energy calibration of the EMCal, and at high p_T (>12 GeV/ c) the cluster-merging effect. The uncertainty on the absolute scale comes from the approximately 1% residual

mismatch between π^0 masses in real data and simulation. This causes a systematic uncertainty that increases gradually from 2% at low p_T , 7% at intermediate p_T , and 9% at the highest momenta. Cluster merging is due to the small opening angle of daughter photons of the high- p_T π^0 , so these photons are reconstructed as a single electromagnetic cluster and the π^0 is lost. The cluster merging effect starts at $p_T > 12$ GeV/ c in PbSc and at $p_T > 16$ GeV/ c in PbGl and results in uncertainty reaching $\approx 20\%$ and $\approx 9\%$ at 20 GeV/ c for π^0 yields, reconstructed in PbSc and PbGl subsystems, respectively. For η mesons, which have a four times larger mass than π^0 , the cluster merging effect would be significant starting at 50 GeV/ c , which is far beyond the p_T range of the η measurement at PHENIX.

For η measurements, the dominant systematic uncertainty comes from the raw yield extraction. The uncertainty is connected to the selection of the invariant-mass distribution analysis parameters such as the fitting range, the background normalization, the polynomial order selection, etc. The maximum difference between the meson yield obtained with the varied parameters and the one obtained with the default parameters is assigned as an uncertainty on raw yield extraction, and it varies from 7% to 12% for the η yields depending on p_T and centrality (see Table III).

Systematic uncertainties for η/π^0 ratios are calculated as a quadratic sum of the type-B uncertainties from π^0 and η yields. Because type-C uncertainties of the π^0 and η yields are 100% correlated between these particle measurements for all p_T , this uncertainty cancels in the ratios. The p_T -correlated systematic uncertainties for R_{AA} include both uncertainties from U + U and $p + p$ measurements [22,36–38]. Examples of total uncertainties of different types for the meson spectra, R_{AA} , and ratios are listed in Table IV.

In π^0 and η measurements, the presented invariant yields are obtained by averaging the PbSc and PbGl results. The averaging uses weights defined by the quadratic sum of

TABLE IV. Total uncertainties for π^0 and η meson spectra, R_{AA} , and η/π^0 ratios at different p_T . The types of uncertainties are described in the text. Values with a range indicate the variation of the uncertainty over the different centrality intervals.

Spectra	Type	2.75 GeV/c	13 GeV/c
π^0 PbSc(PbGl) spectra	Stat	0.3%(0.4%)–0.5%(0.9%)	6%(8%)–20%(14%)
	A	0.8%(1.3%)–1.3%(2.0%)	0.3%(0.4%)–0.4%(0.8%)
	B	6%(7%)–7%(7%)	12%(10%)
	C	5.2%(5.2%)	5.2%(5.2%)
π^0 Combined spectra	Stat	0.2%–0.5%	5%–10%
	A	0.7%–1.1%	0.2%–0.4%
	B	6%	9%–10%
	C	5.2%	5.2%
$\pi^0 R_{AA}$	A + stat	0.8%–1.2%	7%–11%
	B	10%	14%–15%
	C	15%–26%	15%–26%
η PbSc(PbGl) spectra	Stat	6%(9%)–8%(14%)	22%(26%)–32%(36%)
	A	1.2%(2.0%)–3.0%(5.4%)	0.4%(0.7%)–0.9%(1.4%)
	B	13%(13%)–13%(14%)	11%(11%)
	C	5.2%(5.2%)	5.2%(5.2%)
η Combined spectra	Stat	5%–8%	16%–21%
	A	1.2%–3%	0.3%–0.7%
	B	9%–10%	8%–9%
	C	5.2%	5.2%
ηR_{AA}	A + stat	7%–10%	18%–23%
	B	19%	14%
	C	15%–26%	15%–26%
η/π^0	A + stat	5%–8%	17%–22%
	B + C	10%–14%	15%

statistical and uncorrelated systematic uncertainties. Please note that uncertainties, which are correlated between two subsystems (like conversion), were added after the averaging. A comparison between the PbSc(PbGl) spectra uncertainties and the combined ones are shown in Table IV. Data points are plotted at the bin centers rather than the bin-averaged position to facilitate a comparison between different experiments and data sets. To represent the true physical values at the p_T of the bin center, the data have been adjusted to correct for nonlinear effects in bin averaging on a steeply falling spectrum [39].

III. RESULTS AND DISCUSSION

Invariant- p_T spectra for π^0 and η mesons in different U + U collision centrality intervals and MB collisions are shown in Figs. 2(a) and 2(b), respectively. At low p_T the measurements are limited by the rapidly decreasing S/B ratio, and at high p_T by the available statistics. In central U + U collisions π^0 and η yields are measured up to 16 and 14 GeV/c, respectively. At $p_T > 5$ GeV/c the meson spectra are fit to the power-law function

$$f(p_T) = \frac{A}{p_T^n}, \quad (4)$$

where A and n are free parameters. The estimated values of these parameters and the χ^2/NDF values are listed in Table V for each meson species and centrality interval of U + U collisions

The η/π^0 ratios (R_{η/π^0}) as a function of p_T for different U + U centrality intervals are presented in Fig. 3(a). The

comparison of η/π^0 ratios obtained in U + U and Au + Au [40] collisions is shown in Fig. 3(b). Within uncertainties the measured R_{η/π^0} are independent of centrality in the whole p_T range. A constant fit to the MB data at $p_T > 4$ GeV/c for η/π^0 results in $\eta/\pi^0 = 0.476 \pm 0.016$, and the various centrality bins are consistent with this value. Similar results were obtained in hadron-hadron, hadron-nucleus, nucleus-nucleus, and e^+e^- collisions in a wide range of collision energies $\sqrt{s_{NN}} = 3\text{--}2760$ GeV (see, for instance, Refs. [22,41–44]). This suggests that the QGP medium produced in U + U collisions either does not affect the jet fragmentation into light mesons (it is similar as in vacuum) or it affects the π^0 and η the same way, despite their different flavor content.

Figure 4 shows the R_{AA} of π^0 and η mesons as functions of p_T for different U + U centrality intervals. Results are presented only for the Glauber-1 set, the use of the Glauber-2 set will not change the comparison between different meson species. To calculate R_{AA} one needs to use the $p + p$ differential cross sections obtained at the same energy as the A + A yields. RHIC does not have $p + p$ data at $\sqrt{s} = 192$ GeV, thus the meson cross sections at this energy are estimated assuming their power-law dependence on \sqrt{s} , using results at available \sqrt{s} values, as done for charged particles at $\sqrt{s} = 5.02$ TeV in ALICE [45]. For π^0 measurement the interpolation is carried out from the $p + p$ data at $\sqrt{s} = 62.4, 200,$ and 510 GeV. Table VI shows the results of the recalculation.

For η measurements there are no $p + p$ data available at $\sqrt{s} = 62.4$ and 510 GeV, thus the cross sections for these mesons are recalculated from ones at $\sqrt{s} = 200$ GeV [22] using the ratio between the π^0 cross sections at $\sqrt{s} = 192$

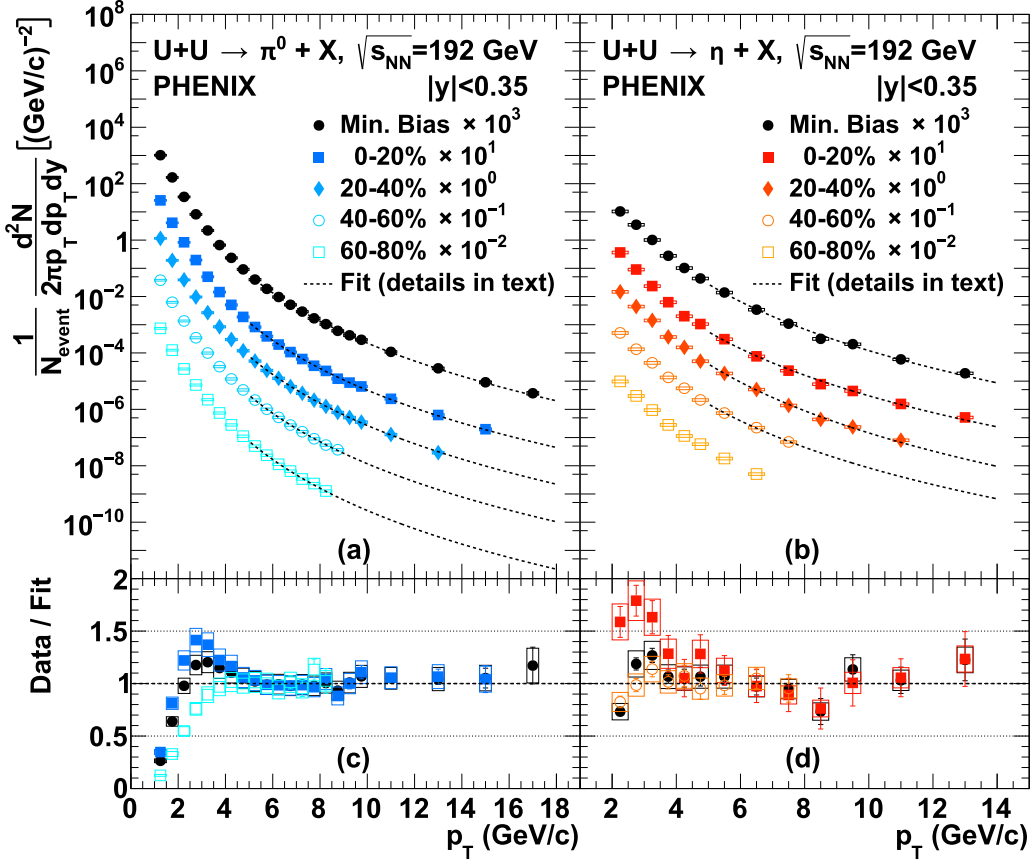


FIG. 2. (a) π^0 and (b) η invariant p_T -spectra measured in different centrality intervals of U + U collisions at $\sqrt{s_{NN}} = 192$ GeV. The dashed curves are fit with a power-law function. Error bars represent a quadratic sum of statistical and type-A systematic uncertainties. Error boxes represent a quadratic sum of type-B and type-C systematic uncertainties. Panels (c) and (d) shows data-to-fit ratios, the markers, error bars, and error boxes are, respectively, the same as for panels (a) and (b).

and 200 GeV. The obtained π^0 and η meson R_{AA} are consistent within uncertainties in the whole p_T range for every analyzed centrality interval of U + U collisions. At $p_T > 5$ GeV/c R_{AA} is $\approx 0.2-0.3$ in the most central collisions. A weak p_T dependence of the measured R_{AA} values can be observed. The suppression of π^0 and η mesons decreases as one moves to more peripheral collisions.

Figure 5 compares R_{AA} of π^0 mesons measured as a function of p_T in $\sqrt{s_{NN}} = 192$ GeV U + U for two Glauber sets

and $\sqrt{s_{NN}} = 200$ GeV Au + Au [23] collisions, plotted for similar N_{part} values. It follows from the N_{coll} values listed in Table I that in peripheral collisions the central values of R_{AA} are slightly different for the Glauber-1 and Glauber-2 models, however, the difference is within experimental uncertainties. The observed π^0 R_{AA} is the same for U + U and Au + Au collisions within uncertainties, which suggests that the π^0 suppression mostly depends on the energy density and size of the produced medium. Note that while the mean N_{part} is

TABLE V. Parameters for the π^0 and η meson invariant transverse momentum spectra fits in U + U collisions at $\sqrt{s_{NN}} = 192$ GeV. Only statistical uncertainties are shown.

Meson	p_T limit	Centrality interval	A	n	χ^2/NDF
$\pi^0 \rightarrow \gamma\gamma$	$p_T > 5$ GeV/c	MB	23.2 ± 1.1	8.02 ± 0.03	20.2/12
		0%–20%	44 ± 3	7.96 ± 0.04	20.6/11
		20%–40%	38 ± 3	8.16 ± 0.04	5.37/11
		40%–60%	13.5 ± 1.8	8.06 ± 0.07	1.90/6
		60%–80%	3.7 ± 1.0	8.15 ± 0.15	3.82/5
$\eta \rightarrow \gamma\gamma$	$p_T > 5$ GeV/c	MB	8.1 ± 2.6	7.83 ± 0.16	8.19/5
		0%–20%	10 ± 6	7.53 ± 0.27	3.65/5
		20%–40%	19 ± 10	8.11 ± 0.26	2.89/4
		40%–60%	2.8 ± 2.4	7.5 ± 0.5	0.41/1

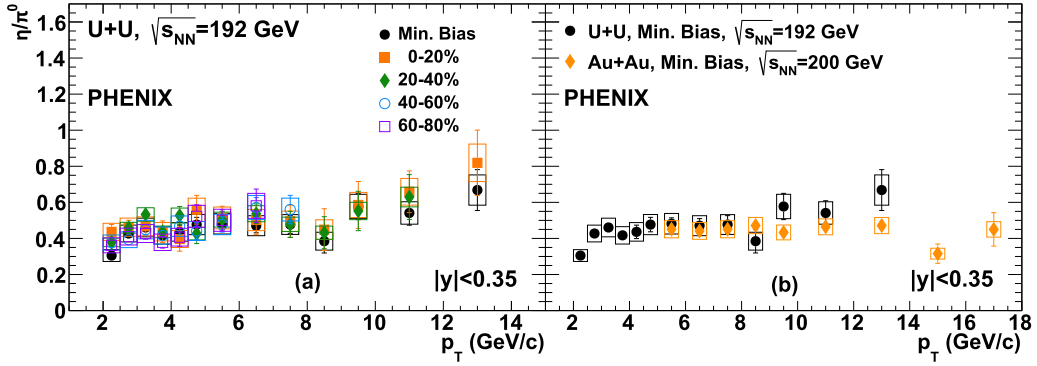


FIG. 3. Panel (a) shows ratios of η and π^0 yields measured as a function of p_T in different centrality intervals of U + U collisions at $\sqrt{s_{NN}} = 192$ GeV. Panel (b) compares η and π^0 yield ratios measured as a function of p_T in MB U + U collisions at $\sqrt{s_{NN}} = 192$ GeV and Au + Au collisions at $\sqrt{s_{NN}} = 200$ GeV [40]. Error bars represent a quadratic sum of statistical and type-A systematic uncertainties for π^0 and η yields. Error boxes represent a quadratic sum of type-B systematic uncertainties from π^0 and η yields.

similar for 40%–60% U + U and 40%–50% Au + Au, its rms is 23.2 for U + U while only 13.1 for Au + Au.

Figure 6 shows the π^0 and η integrated R_{AA} as a function of N_{part} for U + U compared with Au + Au. Figure 6(b) compares π^0 integrated R_{AA} as an N_{part} function between Au + Au and two Glauber sets of U + U. The integration is carried out for $p_T > 5$ GeV/c. Values of obtained integrated R_{AA} are shown in Table VII for different meson species and for Glauber-1 set. The results obtained for the two different collision systems are on a universal trend as a function of N_{part} . The dominant factor in this observable is the size of the

overlap volume (N_{part}), while the much larger fluctuations in U + U because of its shape are secondary.

IV. SUMMARY

PHENIX has measured π^0 and η invariant p_T spectra and R_{AA} in the heaviest collision system available at RHIC, U + U at $\sqrt{s_{NN}} = 192$ GeV in a wide- p_T range ($1 < p_T < 18$ and $2 < p_T < 14$, respectively) and for several centrality intervals. In the more central collisions the spectra are similar to those observed in Au + Au at similar N_{part} (the powers n in

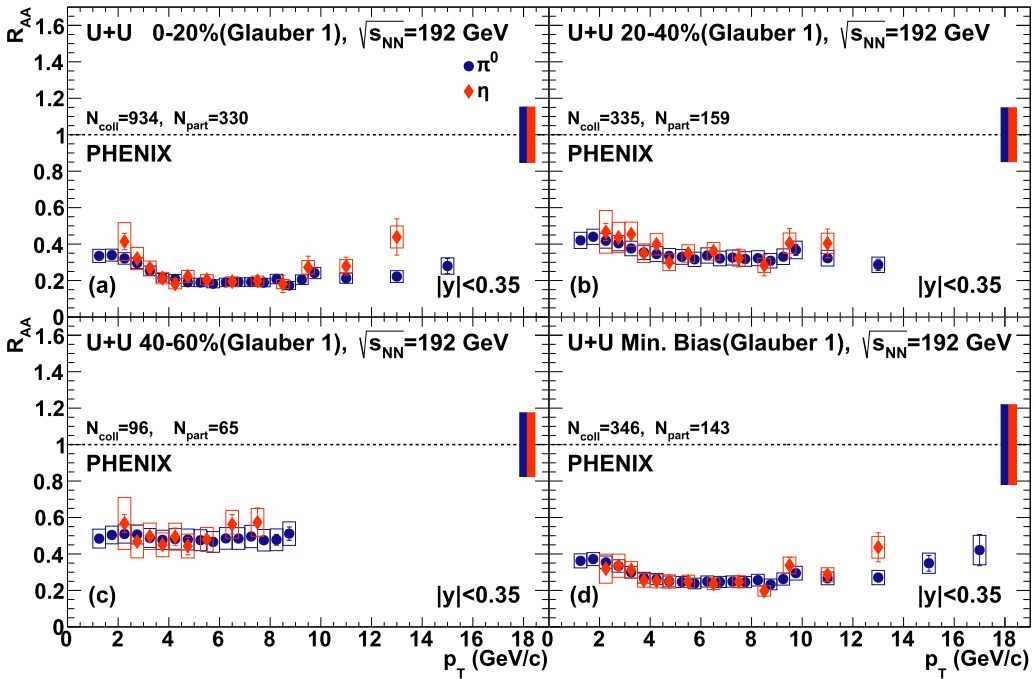


FIG. 4. R_{AA} of π^0 and η mesons measured as a function of p_T in different centrality intervals of U + U collisions at $\sqrt{s_{NN}} = 192$ GeV. Error bars represent a quadratic sum of statistical and type-A systematic uncertainties from U + U and $p + p$ measurements, respectively. Error boxes represent type-B systematic uncertainties from U + U and $p + p$ measurements. Solid and open boxes at unity represent type-C systematic uncertainties from U + U (including uncertainties from the T_{AA} values) and $p + p$, respectively.

TABLE VI. Production cross section of π^0 and η mesons in $p + p$ collisions, recalculated at $\sqrt{s} = 192$ GeV.

Meson decay	p_T (GeV/c)	$Ed^3\sigma/d^3p$ (mb GeV $^{-2}$ c 3)	Stat + Type-A uncertainty	Type-B uncertainty	Type-C uncertainty
$\pi^0 \rightarrow \gamma\gamma$	1.25	3.85×10^{-1}	2.8×10^{-4}	3.76×10^{-2}	3.74×10^{-2}
	1.75	5.97×10^{-2}	7×10^{-5}	4.92×10^{-3}	5.79×10^{-3}
	2.25	1.25×10^{-2}	2.5×10^{-5}	1.03×10^{-3}	1.22×10^{-3}
	2.75	3.16×10^{-3}	1.0×10^{-5}	2.61×10^{-4}	3.06×10^{-4}
	3.25	9.35×10^{-4}	5×10^{-6}	7.8×10^{-5}	9.1×10^{-5}
	3.75	3.12×10^{-4}	2.5×10^{-6}	2.65×10^{-5}	3.02×10^{-5}
	4.25	1.12×10^{-4}	2.4×10^{-7}	1.03×10^{-5}	1.09×10^{-5}
	4.75	4.60×10^{-5}	1.4×10^{-7}	4.24×10^{-6}	4.46×10^{-6}
	5.25	2.02×10^{-5}	8×10^{-8}	1.88×10^{-6}	1.96×10^{-6}
	5.75	9.73×10^{-6}	6×10^{-8}	9.1×10^{-7}	9.4×10^{-7}
	6.25	4.83×10^{-6}	3.5×10^{-8}	4.52×10^{-7}	4.68×10^{-7}
	6.75	2.55×10^{-6}	2.5×10^{-8}	2.40×10^{-7}	2.47×10^{-7}
	7.25	1.44×10^{-6}	1.8×10^{-8}	1.37×10^{-7}	1.40×10^{-7}
	7.75	8.43×10^{-7}	1.3×10^{-8}	8.0×10^{-8}	8.2×10^{-8}
	8.25	5.02×10^{-7}	1.0×10^{-8}	4.8×10^{-8}	4.9×10^{-8}
	8.75	3.19×10^{-7}	7×10^{-9}	3.1×10^{-8}	3.1×10^{-8}
	9.25	1.96×10^{-7}	6×10^{-9}	1.9×10^{-8}	1.9×10^{-8}
	9.75	1.21×10^{-7}	4×10^{-9}	1.2×10^{-8}	1.2×10^{-8}
	11	5.41×10^{-8}	1.4×10^{-9}	5.5×10^{-9}	5.2×10^{-9}
13	1.35×10^{-8}	6×10^{-10}	1.5×10^{-9}	1.3×10^{-9}	
15	3.31×10^{-9}	2.8×10^{-10}	4.0×10^{-10}	3.2×10^{-10}	
17	1.11×10^{-9}	1.5×10^{-10}	1.5×10^{-10}	1.1×10^{-10}	
19	4.8×10^{-10}	1.1×10^{-10}	8×10^{-11}	5×10^{-11}	
$\eta \rightarrow \gamma\gamma$	2.25	3.98×10^{-3}	2.2×10^{-4}	9.2×10^{-4}	3.9×10^{-4}
	2.75	1.28×10^{-3}	7×10^{-5}	2.1×10^{-4}	1.2×10^{-4}
	3.25	3.96×10^{-4}	1.7×10^{-6}	4.41×10^{-5}	3.84×10^{-5}
	3.75	1.33×10^{-4}	8×10^{-7}	1.50×10^{-5}	1.29×10^{-5}
	4.25	4.99×10^{-5}	3.8×10^{-7}	5.73×10^{-6}	4.84×10^{-6}
	4.75	2.14×10^{-5}	2.1×10^{-7}	2.47×10^{-6}	2.08×10^{-6}
	5.5	6.80×10^{-6}	5×10^{-8}	7.0×10^{-7}	6.6×10^{-7}
	6.5	1.76×10^{-6}	2.2×10^{-8}	1.84×10^{-7}	1.71×10^{-7}
	7.5	5.37×10^{-7}	1.1×10^{-8}	5.6×10^{-8}	5.2×10^{-8}
	8.5	1.96×10^{-7}	6×10^{-9}	2.1×10^{-8}	1.9×10^{-8}
	9.5	7.42×10^{-8}	3.2×10^{-9}	7.8×10^{-9}	7.2×10^{-9}
	11	2.52×10^{-8}	1.1×10^{-9}	2.7×10^{-9}	2.4×10^{-9}
	13	5.32×10^{-9}	4.4×10^{-10}	5.7×10^{-10}	5.2×10^{-10}
15	1.66×10^{-9}	2.4×10^{-10}	1.8×10^{-10}	1.6×10^{-10}	
17	5.5×10^{-10}	1.2×10^{-10}	6×10^{-11}	5×10^{-11}	

TABLE VII. Integrated R_{AA} for π^0 and η mesons as a function of N_{part} in U + U collisions at $\sqrt{s_{NN}} = 192$ GeV, calculated for Glauber 1.

Meson	p_T limit	N_{part}	$\langle R_{AA} \rangle$	Stat + Type-A uncertainty	Type-B + Type-C uncertainty
$\pi^0 \rightarrow \gamma\gamma$	$p_T > 5$ GeV/c	17.8	0.61	0.011	0.18
		64.8	0.48	0.005	0.10
		159	0.33	0.0030	0.063
		330	0.19	0.0016	0.037
$\eta \rightarrow \gamma\gamma$	$p_T > 5$ GeV/c	17.8	0.66	0.06	0.19
		64.8	0.52	0.030	0.12
		159	0.35	0.019	0.07
		320	0.22	0.015	0.04

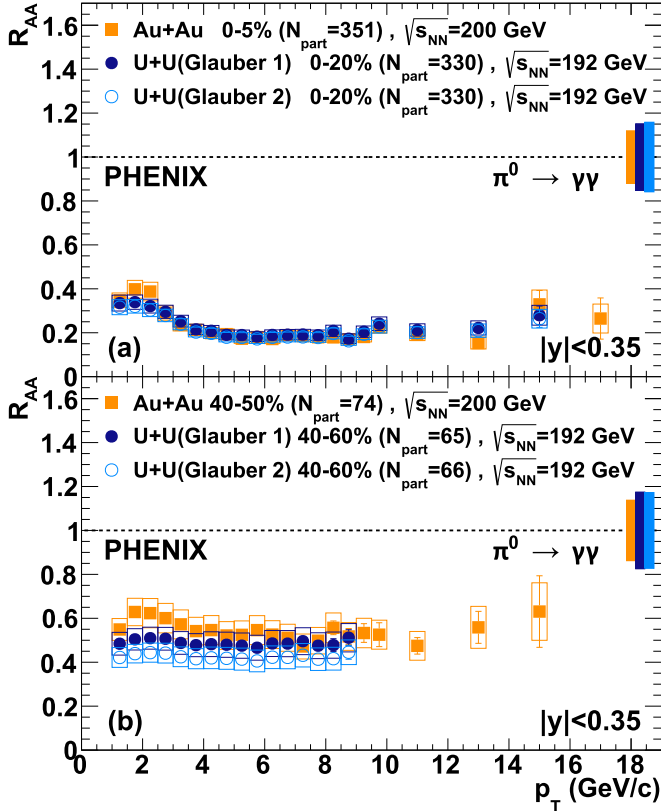


FIG. 5. Comparison at comparable N_{part} of π^0 R_{AA} measured in U + U (two Glauber sets) at $\sqrt{s_{NN}} = 192$ GeV and in Au + Au collisions at $\sqrt{s_{NN}} = 200$ GeV [23]. Error bars represent a quadratic sum of statistical and type-A systematic uncertainties from U + U and $p + p$ measurements. Open boxes are type-B systematic uncertainties for U + U and $p + p$ collisions. The three boxes at unity are type-C systematic uncertainties from $p + p$ and nucleus-nucleus collisions. The boxes from left to right correspond to Au + Au and U + U measurements, respectively. Note that while the mean N_{part} is similar for 40%–60% U + U and 40%–50% Au + Au, its rms is 23.2 for U + U while only 13.1 for Au + Au.

U + U are consistent within fitting errors with the respective fitted powers to Au + Au in Ref. [23]). The values of η/π^0 are independent of collision centrality and p_T and consistent with the previously measured values in hadron-hadron, hadron-nucleus, nucleus-nucleus, as well as e^+e^- collisions at $\sqrt{s_{NN}} = 3\text{--}2760$ GeV, suggesting that either the fragmentation of jets into π^0 and η is unchanged, irrespective of the absence or presence of the medium, or it changes the same way, despite the different flavor content. The values of R_{AA} for π^0 and η are consistent within uncertainties in all analyzed centrality intervals of U + U collisions. The suppression pattern of π^0 in U + U collisions is consistent with Au + Au collisions at the similar interaction energy and similar values of N_{part} , except for $N_{\text{part}} < 100$ and $p_T < 4$ GeV/c (see Fig. 5).

ACKNOWLEDGMENTS

We thank the staff of the Collider-Accelerator and Physics Departments at Brookhaven National Laboratory and the staff

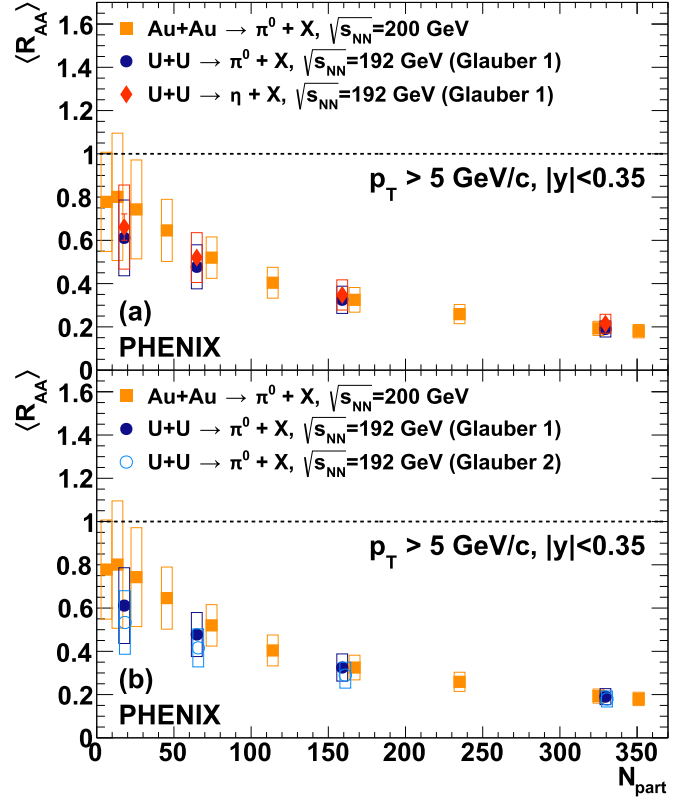


FIG. 6. (a) Comparison of integrated R_{AA} for π^0 and η measured as a function of N_{part} in U + U (Glauber-1 set) and Au + Au collisions at $\sqrt{s_{NN}} = 192$ GeV and $\sqrt{s_{NN}} = 200$ GeV, respectively. (b) Comparison of integrated R_{AA} for π^0 measured as a function of N_{part} in U + U (Glauber-1 and Glauber-2 sets) and Au + Au collisions. Uncertainties are the same as in Fig. 5. The lower limit of integration is $p_T = 5$ GeV/c.

of the other PHENIX participating institutions for their vital contributions. We acknowledge support from the Office of Nuclear Physics in the Office of Science of the Department of Energy, the National Science Foundation, Abilene Christian University Research Council, Research Foundation of SUNY, and Dean of the College of Arts and Sciences, Vanderbilt University (USA), Ministry of Education, Culture, Sports, Science, and Technology and the Japan Society for the Promotion of Science (Japan), Conselho Nacional de Desenvolvimento Científico e Tecnológico and Fundação de Amparo à Pesquisa do Estado de São Paulo (Brazil), Natural Science Foundation of China (People's Republic of China), Croatian Science Foundation and Ministry of Science and Education (Croatia), Ministry of Education, Youth and Sports (Czech Republic), Centre National de la Recherche Scientifique, Commissariat à l'Énergie Atomique, and Institut National de Physique Nucléaire et de Physique des Particules (France), Bundesministerium für Bildung und Forschung, Deutscher Akademischer Austausch Dienst, and Alexander von Humboldt Stiftung (Germany), J. Bolyai Research Scholarship, EFOP, the New National Excellence Program (ÚNKP), NKFIH, and OTKA (Hungary), Department of Atomic Energy and Department of Science and Technology (India), Israel Science Foundation (Israel), Basic Science

Research Program through NRF of the Ministry of Education (Korea), Physics Department, Lahore University of Management Sciences (Pakistan), Ministry of Education and Science, Russian Academy of Sciences, Federal Agency of Atomic Energy (Russia), VR and Wallenberg Foundation

(Sweden), the U.S. Civilian Research and Development Foundation for the Independent States of the Former Soviet Union, the Hungarian American Enterprise Scholarship Fund, the US-Hungarian Fulbright Foundation, and the US-Israel Binational Science Foundation.

-
- [1] I. Arsene *et al.* (BRAHMS Collaboration), Quark gluon plasma and color glass condensate at RHIC? The perspective from the BRAHMS experiment, *Nucl. Phys. A* **757**, 1 (2005).
- [2] B. B. Back *et al.*, The PHOBOS perspective on discoveries at RHIC, *Nucl. Phys. A* **757**, 28 (2005).
- [3] J. Adams *et al.* (STAR Collaboration), Experimental and theoretical challenges in the search for the quark gluon plasma: The STAR Collaboration's critical assessment of the evidence from RHIC collisions, *Nucl. Phys. A* **757**, 102 (2005).
- [4] K. Adcox *et al.* (PHENIX Collaboration), Formation of dense partonic matter in relativistic nucleus-nucleus collisions at RHIC: Experimental evaluation by the PHENIX Collaboration, *Nucl. Phys. A* **757**, 184 (2005).
- [5] S. Chatrchyan *et al.* (CMS Collaboration), Study of high- p_T charged particle suppression in PbPb compared to pp collisions at $\sqrt{s_{NN}} = 2.76$ TeV, *Eur. Phys. J. C* **72**, 1945 (2012).
- [6] B. Abelev *et al.* (ALICE Collaboration), Centrality dependence of charged particle production at large transverse momentum in Pb-Pb collisions at $\sqrt{s_{NN}} = 2.76$ TeV, *Phys. Lett. B* **720**, 52 (2013).
- [7] G. Aad *et al.* (ATLAS Collaboration), Measurement of the jet radius and transverse momentum dependence of inclusive jet suppression in lead-lead collisions at $\sqrt{s_{NN}} = 2.76$ TeV with the ATLAS detector, *Phys. Lett. B* **719**, 220 (2013).
- [8] M. Connors, C. Nattrass, R. Reed, and S. Salur, Jet measurements in heavy ion physics, *Rev. Mod. Phys.* **90**, 025005 (2018).
- [9] J. D. Bjorken, Energy Loss of Energetic Partons in Quark-Gluon Plasma: Possible Extinction of High p_T Jets in Hadron-Hadron Collisions, (1982), FERMILAB-PUB-82-059-THY, FERMILAB-PUB-82-059-T.
- [10] R. Baier, D. Schiff, and B. G. Zakharov, Energy loss in perturbative QCD, *Annu. Rev. Nucl. Part. Sci.* **50**, 37 (2000).
- [11] X.-N. Wang, M. Gyulassy, and M. Plumer, The LPM effect in QCD and radiative energy loss in a quark gluon plasma, *Phys. Rev. D* **51**, 3436 (1995).
- [12] A. Majumder, B. Muller, and X.-N. Wang, Small Shear Viscosity Of A Quark-Gluon Plasma Implies Strong Jet Quenching, *Phys. Rev. Lett.* **99**, 192301 (2007).
- [13] G.-Y. Qin, J. Ruppert, C. Gale, S. Jeon, G. D. Moore, and M. G. Mustafa, Radiative And Collisional Jet Energy Loss In The Quark-Gluon Plasma At RHIC, *Phys. Rev. Lett.* **100**, 072301 (2008).
- [14] X.-F. Chen, T. Hirano, E. Wang, X.-N. Wang, and H. Zhang, Suppression of high p_T hadrons in Pb + Pb Collisions at LHC, *Phys. Rev. C* **84**, 034902 (2011).
- [15] C. Young, B. Schenke, S. Jeon, and C. Gale, MARTINI event generator for heavy quarks: Initialization, parton evolution, and hadronization, *Phys. Rev. C* **86**, 034905 (2012).
- [16] A. Majumder and C. Shen, Suppression of the High p_T Charged Hadron R_{AA} at the LHC, *Phys. Rev. Lett.* **109**, 202301 (2012).
- [17] J. Xu, A. Buzzatti, and M. Gyulassy, Azimuthal jet flavor tomography with CUJET2.0 of nuclear collisions at RHIC and LHC, *J. High Energy Phys.* **08** (2014) 063.
- [18] M. L. Miller, K. Reygers, S. J. Sanders, and P. Steinberg, Glauber modeling in high energy nuclear collisions, *Annu. Rev. Nucl. Part. Sci.* **57**, 205 (2007).
- [19] B. Schenke, P. Tribedy, and R. Venugopalan, Initial-state geometry and fluctuations in Au + Au, Cu + Au, and U + U collisions at energies available at the BNL Relativistic Heavy Ion Collider, *Phys. Rev. C* **89**, 064908 (2014).
- [20] K. Adcox *et al.* (PHENIX Collaboration), Suppression Of Hadrons With Large Transverse Momentum In Central Au + Au Collisions At $\sqrt{s_{NN}} = 130$ GeV, *Phys. Rev. Lett.* **88**, 022301 (2002).
- [21] J. Adams *et al.* (STAR Collaboration), Transverse Momentum And Collision Energy Dependence Of High p_T Hadron Suppression In Au + Au Collisions At Ultrarelativistic Energies, *Phys. Rev. Lett.* **91**, 172302 (2003).
- [22] S. S. Adler *et al.* (PHENIX Collaboration), High transverse momentum η meson production in $p + p$, $d + Au$ and Au + Au collisions at $\sqrt{s_{NN}} = 200$ GeV, *Phys. Rev. C* **75**, 024909 (2007).
- [23] A. Adare *et al.* (PHENIX Collaboration), Suppression Pattern of Neutral Pions at High Transverse Momentum in Au + Au Collisions at $\sqrt{s_{NN}} = 200$ GeV and Constraints on Medium Transport Coefficients, *Phys. Rev. Lett.* **101**, 232301 (2008).
- [24] A. Adare *et al.* (PHENIX Collaboration), Evolution of π^0 Suppression in Au + Au Collisions From $\sqrt{s_{NN}} = 39$ to 200 GeV, *Phys. Rev. Lett.* **109**, 152301 (2012); **125**, 049901 (2020).
- [25] A. Adare *et al.* (PHENIX Collaboration), Onset of π^0 Suppression Studied in Cu + Cu Collisions at $\sqrt{s_{NN}} = 22.4$, 62.4, and 200 GeV, *Phys. Rev. Lett.* **101**, 162301 (2008).
- [26] A. Adare *et al.* (PHENIX Collaboration), Transverse momentum dependence of meson suppression η suppression in Au + Au collisions at $\sqrt{s_{NN}} = 200$ GeV, *Phys. Rev. C* **82**, 011902 (2010).
- [27] K. Adcox *et al.* (PHENIX Collaboration), PHENIX detector overview, *Nucl. Instrum. Methods Phys. Res., Sect. A* **499**, 469 (2003).
- [28] M. Allen *et al.* (PHENIX Collaboration), PHENIX inner detectors, *Nucl. Instrum. Methods Phys. Res., Sect. A* **499**, 549 (2003).
- [29] A. Adare *et al.* (PHENIX Collaboration), Forward J/ψ production in U + U collisions at $\sqrt{s_{NN}} = 193$ GeV, *Phys. Rev. C* **93**, 034903 (2016).
- [30] L. Adamczyk *et al.* (STAR Collaboration), Azimuthal Anisotropy in U + U and Au + Au Collisions at RHIC, *Phys. Rev. Lett.* **115**, 222301 (2015).

- [31] M. H., B. Mohanty, and N. Xu, Predictions of elliptic flow and nuclear modification factor from 200 GeV U + U collisions at RHIC, *Phys. Lett. B* **679**, 440 (2009).
- [32] Q. Y. Shou, Y. G. Ma, P. Sorensen, A. H. Tang, F. Videbæk, and H. Wang, Parameterization of deformed nuclei for glauber modeling in relativistic heavy ion collisions, *Phys. Lett. B* **749**, 215 (2015).
- [33] L. Aphecetche *et al.* (PHENIX Collaboration), PHENIX calorimeter, *Nucl. Instrum. Methods Phys. Res., Sect. A* **499**, 521 (2003).
- [34] R. Brun, R. Hagelberg, M. Hansroul, and J. C. Lassalle, “GEANT: Simulation Program for Particle Physics Experiments. User Guide and Reference Manual” (1978), CERN-DD-78-2-REV.
- [35] A. Adare *et al.* (PHENIX Collaboration), Quantitative constraints on the opacity of hot partonic matter from semi-inclusive single high transverse momentum pion suppression in Au + Au collisions at $\sqrt{s_{NN}} = 200$ GeV, *Phys. Rev. C* **77**, 064907 (2008).
- [36] A. Adare *et al.* (PHENIX Collaboration), Inclusive cross section and double helicity asymmetry for π^0 production in $p + p$ collisions at $\sqrt{s} = 62.4$ GeV, *Phys. Rev. D* **79**, 012003 (2009).
- [37] A. Adare *et al.* (PHENIX Collaboration), Inclusive cross-section and double helicity asymmetry for π^0 production in $p + p$ collisions at $\sqrt{s} = 200$ GeV: Implications for the polarized gluon distribution in the proton, *Phys. Rev. D* **76**, 051106 (2007).
- [38] A. Adare *et al.* (PHENIX Collaboration), Inclusive cross section and double-helicity asymmetry for π^0 production at midrapidity in $p + p$ collisions at $\sqrt{s} = 510$ GeV, *Phys. Rev. D* **93**, 011501 (2016).
- [39] G. D. Lafferty and T. R. Wyatt, Where to stick your data points: The treatment of measurements within wide bins, *Nucl. Instrum. Methods Phys. Res., Sect. A* **355**, 541 (1995).
- [40] A. Adare *et al.* (PHENIX Collaboration), Neutral pion production with respect to centrality and reaction plane in Au + Au collisions at $\sqrt{s_{NN}} = 200$ GeV, *Phys. Rev. C* **87**, 034911 (2013).
- [41] F. W. Busser *et al.*, A study of high transverse momentum η and π^0 mesons at the CERN ISR collaboration, *Phys. Lett. B* **55**, 232 (1975).
- [42] L. Apanasevich *et al.* (Fermilab E706 Collaboration), Production of π^0 and η mesons at large transverse momenta in pp and pBe Interactions at 530 and 800 GeV/c. *Phys. Rev. D* **68**, 052001 (2003).
- [43] C. Aidala *et al.* (PHENIX Collaboration), Production of π^0 and η mesons in Cu + Au collisions at $\sqrt{s_{NN}} = 200$ GeV, *Phys. Rev. C* **98**, 054903 (2018).
- [44] S. Acharya *et al.* (ALICE Collaboration), Neutral pion and η meson production at mid-rapidity in Pb-Pb collisions at $\sqrt{s_{NN}} = 2.76$ TeV, *Phys. Rev. C* **98**, 044901 (2018).
- [45] B. Abelev *et al.* (ALICE Collaboration), Transverse Momentum Distribution and Nuclear Modification Factor of Charged Particles in p -Pb Collisions at $\sqrt{s_{NN}} = 5.02$ TeV, *Phys. Rev. Lett.* **110**, 082302 (2013).